Solution Structures of the N-Terminal Domain of Yeast Calmodulin: Ca^{2+}-Dependent Conformational Change and Its Functional Implication‡

Hiroaki Ishida,§,|| Kiyohiro Takahashi,§,|| Ken-ichi Nakashima,⊥ Yasuhiro Kumaki,# Mitsuo Nakata,§ Kunio Hikichi,§ and Michio Yazawa*,⊥

Divisions of Biological Sciences, Chemistry, and High-Resolution NMR Laboratory, Graduate School of Science, Hokkaido University, Sapporo 060-0810, Japan

Received March 14, 2000; Revised Manuscript Received June 19, 2000

ABSTRACT: We have determined solution structures of the N-terminal half domain (N-domain) of yeast calmodulin (YCM0-N, residues 1−77) in the apo and Ca^{2+}-saturated forms by NMR spectroscopy. The Ca^{2+}-binding sites of YCM0-N consist of a pair of helix-loop-helix motifs (EF-hands), in which the loops are linked by a short β-sheet. The binding of two Ca^{2+} causes large rearrangement of the four α-helices and exposes the hydrophobic surface as observed for vertebrate calmodulin (CaM). Within the observed overall conformational similarity in the peptide backbone, several significant conformational differences were observed between the two proteins, which originated from the 38% disagreement in amino acid sequences. The β-sheet in apo YCM0-N is strongly twisted compared with that in the N-domain of CaM, while it turns to the normal more stable conformation on Ca^{2+} binding. YCM0-N shows higher cooperativity in Ca^{2+} binding than the N-domain of CaM, and the observed conformational change of the β-sheet is a possible cause of the highly cooperative Ca^{2+} binding. The hydrophobic surface on Ca^{2+}-saturated YCM0-N appears less flexible due to the replacements of Met51, Met71, and Val55 in the hydrophobic surface of CaM with Leu51, Leu71, and Ile55, which is thought to be one of reasons for the poor activation of target enzymes by yeast CaM.

Calmodulin (CaM)[1] is a ubiquitous intracellular Ca^{2+}-receptor protein, which can activate various Ca^{2+}-dependent enzymes in response to transient Ca^{2+} influx caused by extracellular stimuli. The X-ray crystal structure of Ca^{2+}-saturated CaM resembles a dumbbell in which two globular domains (N- and C-domain) are linked by an α-helix (*1*, *2*). Each domain contains two Ca^{2+}-binding sites and consists of a pair of EF-hand helix-loop-helix motifs (*3*), in which the two loops are joined by a short antiparallel β-sheet. The EF-hand motifs are referred to as EF1, EF2, EF3, and EF4 from the N-terminus. The helical linker connecting two domains is highly flexible in solution while each domain behaves as an independent Ca^{2+}-binding unit (*4*, *5*). NMR studies (*6*, *7*) showed that each domain of apo CaM has the same secondary structure elements as those observed for Ca^{2+}-saturated CaM. The four helices in the pair of EF-hand motifs in apo CaM, however, form a characteristic bundle, and the cluster of hydrophobic side chains is not exposed to solvent. In the X-ray crystal structure of Ca^{2+}-saturated CaM, these helices are rearranged, and the hydrophobic residues are exposed to solvent (*1*, *2*). The resulting hydrophobic surfaces in the both domains play essential roles for recognition of target proteins (*8*−*11*). Many Met residues are in the exposed hydrophobic surfaces (*1*, *2*), and the conformational flexibility of their side chains is important for the broad sequence specificity of CaM in target recognition (*12*−*15*).

Amino acid sequences of CaMs isolated from vertebrates, scallop, and drosophila are very similar with their identity of more than 90% (*16*). Amino acid sequence of CaM from yeast, *Saccharomyces cerevisiae* (146 amino acid residues) is, however, only about 60% identical to those of other CaMs (*17*−*19*), and yeast CaM shows characteristic Ca^{2+} binding and other functional properties. Hereafter, we refer to calmodulin from vertebrate, scallop, and drosophila as CaM, and calmodulin from yeast as YCM0. YCM0 binds only 3 mol of Ca^{2+} instead of 4, since Ca^{2+} cannot bind to a site in YCM0 corresponding to EF4 of CaM (*18*). The N-domain of YCM0 (YCM0-N, residues 1−77 containing EF1 and

‡ Coordinates for the 30 NMR structures of apo and Ca^{2+}-bound N-terminal domain of yeast calmodulin have been deposited at the Brookhaven Protein Data Bank (accession numbers 1F54 and 1F55).

* To whom correspondence should be addressed. Division of Chemistry, Graduate School of Science, Hokkaido University. Fax: 81-11-706-4924. E-mail: myazawa@sci.hokudai.ac.jp.

§ Division of Biological Sciences.

|| These authors contributed equally to this work.

⊥ Division of Chemistry.

High-Resolution NMR Laboratory.

[1] Abbreviations: CaM, calmodulin; skMLCK, skeletal muscle myosin light chain kinase; smMLCK, smooth muscle myosin light chain kinase; PDE, cyclic nucleotide phosphodiesterase; CaN, calcineurin; CaMKII, calmodulin dependent protein kinase type II; 2D, two-dimensional; 3D, three-dimensional; DANTE, delays alternating with nutation for tailored excitation; DQF−COSY, double quantum filtered correlation spectroscopy; HSQC, heteronuclear single quantum coherence spectroscopy; NMR, nuclear magnetic resonance; NOE, nuclear Overhauser effect; NOESY, nuclear Overhauser effect spectroscopy; PFG, pulsed field gradient; TOCSY, total correlation spectroscopy; TSP, 2,2,3,3-tetradeutero-3-(tri-methylsilyl)propionic acid sodium salt; YCM0, yeast calmodulin; YCM0-N, N-terminal half domain of yeast calmodulin; $d_{NN}(i-x,i)$, NOE cross-peak between amide protons of residue $i - x$ and i; $d_{\alpha N}(i-x,i)$, NOE cross-peaks between α proton of residue $i - x$ and amide proton of residue i; $d_{\beta N}(i-x,i)$, NOE cross-peaks between β protons of residue $i - x$ and amide proton of residue i.

10.1021/bi000582x CCC: $19.00
Published on Web 10/21/2000

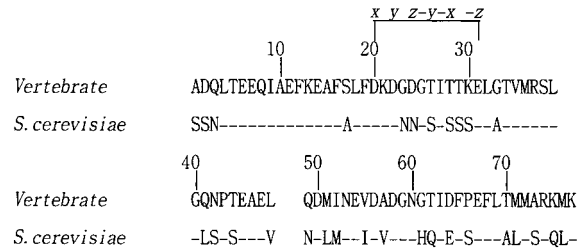

FIGURE 1: Alignment of the amino acid sequence of the N-domain of vertebrate CaM (residues 1−77) (top) with the one of YCM0-N (bottom). In the sequence of YCM0-N, only substituted residues are indicated, and identical residues are indicated by dashes. Positions of the six residues coordinating Ca^{2+} in EF1 and EF2 are indicated by *x*, *y*, *z*, −*y*, −*x*, and −*z*.

EF2) can bind two Ca^{2+} in a highly cooperative manner like the C-domain of CaM containing EF3 and EF4 can do (*20*). YCM0 can activate target enzymes from vertebrates such as phosphodiesterase (PDE) and myosin light chain kinase (MLCK), but the resulting activities are very poor (*18*, *21*). However, the activation of calcineurin (CaN) from vertebrate by YCM0 is not so poor compared with that by CaM (K.N. and M.Y., unpublished results).

Despite such characteristic properties of YCM0, the analysis of NMR spectra has showed that the structure is principally similar to that of CaMs (*19*, *22*). It implies that rather small conformational differences from vertebrate CaM in addition to interactions between two-half-molecular domains of YCM0 (*20*) give rise to the different properties. Here, we describe solution structures of YCM0-N in the apo and the Ca^{2+}-saturated forms determined by two- and three-dimensional NMR techniques. We discuss structural differences between YCM0-N and the N-domain of CaM. The relation between the conformation of YCM0-N and the highly cooperative Ca^{2+} binding compared with that of the N-domain of CaM is also discussed. Moreover, we propose a reason for the limited levels of activation of target enzymes by YCM0.

MATERIALS AND METHODS

Sample Preparation. A recombinant protein, YCM0-N (Ser1−Lys77, Figure 1), corresponding to the N-domain of yeast, *Saccharomyces cerevisiae*, CaM (YCM0) was overexpressed in *Escherichia coli* (strain TG1) containing expression plasmid pYCM0-N, which was constructed from plasmid pYCM0 (*23*, *24*) by replacing a codon TCA for Ser78 of YCM0 with a stop codon TGA. In later experiments, YCM0-N was expressed in *E. coli* strain BL21 (DE3) transformed with plasmid pETYCM0-N. For construction of pETYCM0-N, an *Nde*I site was generated at the initiation codon for YCM0-N in plasmid pYCM0-N and the resulting plasmid was digested with *Nde*I/*Bam*HI. Then, the cDNA fragment coding for YCM0-N was inserted into the *Nde*I/*Bam*HI site of plasmid pET-30b(+) (Novagene) generating plasmid pETYCM0-N. Uniformly ^{15}N-labeled recombinant YCM0-N was obtained by growing cells in M10 minimal medium containing $^{15}NH_4Cl$ (0.5 g/1 L) (*25*). YCM0-N was purified using a previously published method (*23*−*24*, *26*). We obtained Ca^{2+}-free YCM0-N using a Sephadex G-25 gel column.

NMR Experiments. Samples were dissolved in 0.3 mL of 90% H_2O/10% D_2O or 99.99% D_2O solution containing 50 mM KCl and 0.02% NaN_3. The pH/pD values of the samples were adjusted to 6.8 ± 0.1 by adding KOD without consideration of the isotope effects. Sample concentrations of the apo-form were 3 mM. For the Ca^{2+}-form, sample concentrations were 5 mM for nonlabeled H_2O sample and 3 mM for nonlabeled D_2O sample, and for ^{15}N-labeled sample. Three-fold molar excess $CaCl_2$ over protein was added to each sample of Ca^{2+}-form.

All NMR experiments were performed using JEOL JNM-A600 and A500 spectrometers at ^1H frequencies of 600 and 500 MHz, respectively. Each spectrometer is equipped with a triple resonance probe-head with a *z*-axis pulse field gradient coil. Temperature was kept at 30 ± 0.1 °C throughout the experiments. The chemical shifts of ^1H and ^{15}N resonances are reported from the internal standard TSP (0 ppm) and external standard $^{15}NH_4Cl$ (24.93 ppm), respectively.

2D-NMR data of DQF−COSY (*27*), NOESY (*28*, *29*), and TOCSY (*30*, *31*) were acquired with 1024 complex t_2 points and 512 complex t_1 points. Mixing times of 100 and 150 ms were used for the 2D-NOESY spectra. Water peak suppression was achieved by DANTE (*32*) for DQF−COSY and TOCSY, and by WATERGATE (*33*) for NOESY.

^{15}N-edited 3D-NOESY−HSQC (*34*, *35*) data and ^{15}N-edited 3D-TOCSY−HSQC (*34*, *36*) data were collected with 128, 32, and 256 complex points, respectively, for t_1 (H), t_2 (^{15}N), and t_3 (NH) time domains. A mixing time of 150 ms was used in the ^{15}N-edited 3D-NOESY−HSQC spectra. MLEV times for 2D-TOCSY and ^{15}N-edited 3D-TOCSY−HSQC was 75 ms. Spectral widths of ^1H and ^{15}N resonances were 8000 and 1800 Hz, respectively. Water peak suppression was achieved by field gradient pulse in all 3D-NMR experiments.

{^1H-^{15}N}-HSQC spectra were used to identify slowly exchanging amide protons. HSQC data were acquired with 1024 complex t_2 points and 256 complex t_1 points. Data acquisitions for the HSQC spectra were started at 1, 9, 25, 57, 121, 249, and 505 min after dissolving the protein in D_2O. The experiment was carried out at room temperature.

Data processing and analysis were performed using NMRPipe (*37*) and/or Felix 95.0 software package (Molecular Simulations Inc., San Diego, CA) on a SGI O2 workstation (Silicon Graphics, Mountain View, CA).

Structural Calculations. The assigned NOE cross-peaks in the apo-form were broadly classified on the basis of peak intensity into strong, medium, and weak, which were assumed to correspond to distances of 1.8−3.0 (1.8−3.5 for HN), 1.8−4.0 (1.8−4.5 for HN), and 1.8−5.9 Å, respectively. All of NOE cross-peaks in the Ca^{2+}-form were grouped on the basis of peak intensity into 1.8−3.7, 1.8−4.7, and 1.8−5.9 Å. φ-Torsion angle restraints were derived from $^3J_{NH-H\alpha}$ coupling constants and the Karplus curve. Values of −60 ± 30 and −120 ± 50° were used, respectively, for residues with $^3J_{NH-H\alpha}$ values <6 and >9 Hz. The hydrogen bond restraints were used in the later stage of structural determination. The available hydrogen bonds were determined based on slowly exchanging backbone amide protons and the calculated structures without hydrogen bond restraints. The hydrogen bond distances of NH−O in α-helix and NH−O in β-sheet were set to 1.8−2.3 and 2.3−3.3 Å, respectively. Calcium-ligand distance restraints were set to 2.4−2.8 Å on the basis of EF-hand model of Strynadka and

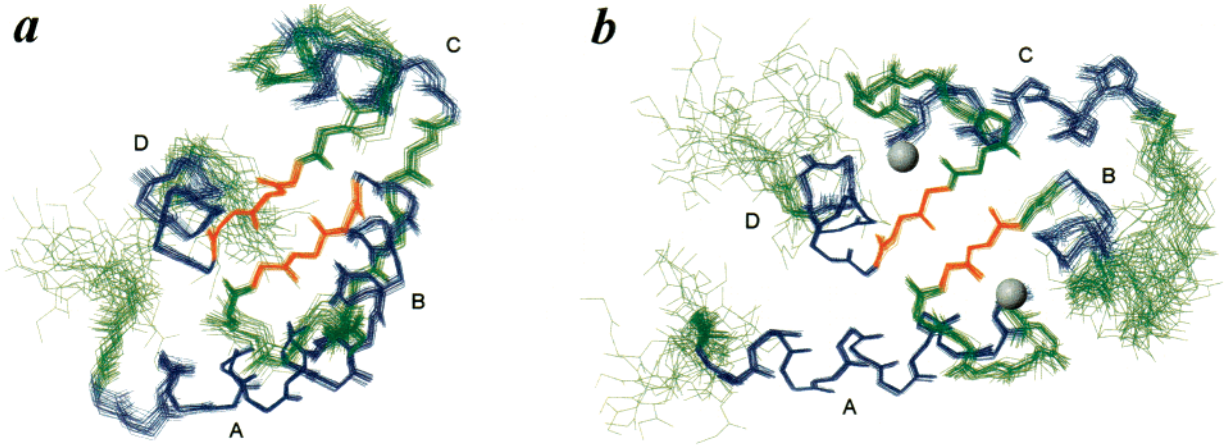

FIGURE 2: Solution structures of YCM0-N. Best-fit superpositions of the backbone heavy atoms of the 30 NMR structures of YCM0-N are shown. (a) The structures of apo YCM0-N were superimposed using the folding regions except for loop and linker regions (residues 6−18, 26−39, 45−53, and 62−72). (b) The structures of Ca^{2+}-bound YCM0-N were superimposed using the folding regions except for the Linker and ill-determined regions (residues 6−33 and 45−72). The region of helices and sheets are shown in blue and red, respectively. The position of Ca^{2+} in the average structure is shown as spheres. Helices are labeled as described in the text.

James (*38*). The distances from Ca^{2+} to five protein ligands (x, y, z, $-y$, and $-z$) out of six (a ligand of $-x$ is water) were employed.

Structure calculation was performed using X-PLOR version 3.851 (*39*). Two hundred starting structures were generated from an extended conformation using an ab initio simulated annealing (SA) protocol (sa.inp) (*40*) and refined by a rapid SA protocol (refine.inp). Structures with distance violations greater than 0.2 Å and dihedral angle violations greater than 2° were cut off by accept.inp. The parameter files parallhdg.pro and topallhdg.pro were used to define the force constants and topologies, respectively for apo-form structure. For the calculation of Ca^{2+}-form structures, parallhdg.pro and topallhdg.pro supplemented with parameters for calcium were used. An average structure was generated by calculating mean atom positions of the 30 lowest-energy simulated annealing structures with average.inp. Geometric strain of this average structure was removed by restrained energy minimization. Solvent-accessible surface areas were calculated with X-PLOR using a water probe radius of 1.4 Å. Insight II (Molecular Simulations Inc., San Diego, CA), MOLMOL program (*41*), and WebLav VeiwerLite (Molecular Simulations Inc., San Diego, CA) were used for structural drawing.

RESULTS AND DISCUSSION

Structural Determination of YCM0-N. The chemical shift assignments for both apo and Ca^{2+}-saturated YCM0-N were performed by the standard method using DQF−COSY, NOESY, TOCSY, ^{15}N-edited 3D-NOESY, and TOCSY spectra (*42*). Stereospecific information was not included throughout our structural determinations. Spin systems were classified on the basis of connectivities between main-chain amide and side-chain protons observed in 2D-TOCSY and ^{15}N-edited 3D-TOCSY spectra. These spin systems were connected using sequence-specific NOEs, $d_{NN}(i-1, i)$, $d_{\alpha N}(i-1, i)$, and $d_{\beta N}(i-1, i)$ derived from 2D-NOESY and ^{15}N-edited 3D-NOESY spectra. In {^{1}H-^{15}N}-HSQC spectra, total of 73 and 70 of 75 amide peaks except for one Pro were identified for apo and Ca^{2+}-saturated YCM0-N, respectively. The {^{1}H-^{15}N}-HSQC spectrum of YCM0-N in the apo-form was well consistent with assigned HSQC spectrum of intact YCM0 in the apo form (unpublished results) except for signals from the C-terminal residues, Gln75, Leu76, and Lys77, with a maximum ^{15}N chemical shift difference of 0.40 ppm. Thus, the conformation of YCM0-N is the same as the one of the N-domain in YCM0. Total of 64 and 17 $^3J_{NH-H\alpha}$ coupling constants, respectively, for apo and Ca^{2+}-saturated YCM0-N were obtained using DQF−COSY to provide dihedral angle restraints.

The structures of apo and Ca^{2+}-saturated YCM0-N were determined using 996 and 920 restraints, respectively, derived from the present experiments. In the apo form, the experimental restraints include 917 interproton distances derived from NOEs, 44 φ dihedral angles, and 35 hydrogen bonding. In the Ca^{2+}-saturated form, the experimental restraints include 863 interproton distances derived from NOEs, 17 φ dihedral angles, 28 hydrogen bonding, and 12 calcium-ligand distances. A total of 200 simulated annealing structures were generated and in final 30 structures with lowest energies and without violations greater than 0.2 Å and 2° were determined for each of apo and Ca^{2+}-saturated YCM0-N. Figure 2 show best-fit superposition of the backbone atoms for apo and Ca^{2+}-saturated YCM0-N, respectively. The average root-mean-square deviations (rmsd) for backbone heavy atoms (N, C_α, C, O) in the folding regions (residues 6−72) of apo YCM0-N were 0.58 ± 0.13 Å. The average rmsd for backbone heavy atoms in the folding regions of Ca^{2+}-saturated YCN0-N except for the linker and ill-determined regions (residues 6−33, and 45−72, respectively) was 0.51 ± 0.10 Å. The φ and ψ angles of the peptide backbone in the folding regions of YCM0-N in the two forms were checked by a program PROCHECK (*43*) and all angles were found within allowed regions of a Ramachandran map. A summary of geometric and energetic statistics of the final structures is given in Table 1 and the structural data for apo and Ca^{2+}-saturated YCM0-N were plotted as a function of residue number (Figure 3).

Structure of YCM0-N. Figure 4, panels a and b, show the best-fit superpositions of structures of apo and Ca^{2+}-saturated YCM0-N to those of the N-domain of CaM in the apo and Ca^{2+}-saturated states: The values of backbone rmsd are 1.72

Table 1: Structural Statistics of the 30 Structures of Apo and Ca^{2+}-Saturated YCM0-N

Restraints for Structure Calculation		
	apo-form	Ca^{2+}-form
total restraints used	996	920
total NOE restraints	917	863
intraresidue	157	223
sequential	249	226
medium range	273	225
long range	238	189
hydrogen bond restraints	35	28
φ torsion angle restraints	44	17
Ca^{2+}-ligand distance restraints	0	12
distance restraint violations greater than 0.2 Å	0	0
φ torsion angle restraint violations greater than 2°	0	0
rmsd from Idealized Geometry		
bonds (Å)	$(0.92 \times 10^{-3}) \pm (0.53 \times 10^{-5})$	$(1.25 \times 10^{-3}) \pm (3.69 \times 10^{-5})$
bond angles (deg)	$(0.45 \pm 0.51) \times 10^{-3}$	$(0.47 \pm 2.11) \times 10^{-3}$
improper torsions (deg)	$(0.36 \pm 0.32) \times 10^{-3}$	$(0.37 \pm 2.89) \times 10^{-3}$
rmsd from Experimental Restraints		
distance (Å)	$(3.36 \times 10^{-3}) \pm (0.15 \times 10^{-3})$	$(9.56 \times 10^{-3}) \pm (0.34 \times 10^{-3})$
dihedral angle (deg)	$(2.15 \times 10^{-3}) \pm (2.62 \times 10^{-3})$	$(8.38 \times 10^{-2}) \pm (4.30 \times 10^{-2})$
X-PLOR potential energy (E_{total}) (kcal mol^{-1})	77.72 ± 0.20	95.00 ± 1.31

PROCHECK Ramachandran Plot Statistics	residues (6−72)	residues (6−72)
residues in most favored regions (%)	78.9	70.4
residues in additional allowed regions (%)	21.1	23.9
residues in generously allowed regions (%)	0.0	5.6
residues in disallowed regions (%)	0.0	0.0

rmsd of Backbone Heavy Atoms (N, C_α, C, and O)	
apo-form	
residues 6−18, 26−39, 45−53, 62−72	0.47 ± 0.15 Å
Ca^{2+}-form	
residues 6−72	0.58 ± 0.13 Å
residues 6−33, 45−72	0.51 ± 0.10 Å
residues 6−72	1.04 ± 0.29 Å

rmsd of All Heavy Atoms	
apo-form	
residues 6−18, 26−39, 45−53, 62−72	1.19 ± 0.14 Å
residues 6−72	1.27 ± 0.11 Å
Ca^{2+}-form	
residues 6−33, 45−72	1.16 ± 0.09 Å
residues 6−72	1.71 ± 0.35 Å

$\pm$ 0.05 and 1.35 $\pm$ 0.06 Å in the apo and Ca^{2+}-saturated forms, respectively; apo and Ca^{2+}-saturated YCM0-N are almost in the same conformation as the N-terminal domain of apo and Ca^{2+}-saturated CaM, respectively. Thus, YCM0-N has four helices and a short antiparallel β-sheet (Figure 2). Using the Kabsch and Sander algorithm (*44*) for ensemble of 30 NMR conformers of apo and Ca^{2+}-saturated YCM0-N, following elements of the secondary structure were detected in most of conformers. Four helices in the apo form are residues 6−18 (A-helix), 29−39 (B-helix), 45−53 (C-helix), and 65−72 (D-helix). In the Ca^{2+}-saturated form, the region corresponding to the last part of B-helix in the apo form is not determined well, and most of conformers assume irregular helical conformation (Figure 2); as a result, four helices are residues 6−19 (A-helix), 29−33 (B-helix), 45−55 (C-helix), and 65−72 (D-helix). In both forms, A- and B-helices, and C- and D-helices form EF-hand motifs, EF1 and EF2, respectively. These two EF-hand motifs of both forms are connected by a short antiparallel β-sheet (residues 26−28 and 62−64); the hydrogen bonds are formed between residues Ile27 and Ile63.

A- and D-helices are well-defined as inferred from the existence of a large number of NOEs in both structures. In particular, we found a large number of interhelical NOEs for ring protons of Phe residues which are located in A- and D-helices (Phe12, 16, 19, 65, and 68) (Figure 3a). The positions of Phe residues in the amino acid sequence are exactly the same as those of CaM (Figure 1), and these residues form a so-called aromatic box: a hydrophobic core found in all CaMs and other EF-hand domains.

In the apo form, many hydrophobic residues in B-helix interact with the aromatic box. As a result, B-helix is also well-defined in the apo form due to many NOEs including helix-specific NOEs, $d_{NN}(i-2,i)$, $d_{\alpha N}(i-3,i)$, and $d_{\alpha N}(i-4,i)$ and many interhelical NOEs with A- and D-helices. However, in the Ca^{2+}-form, the region corresponding to the C-terminal part of B-helix in the apo form was not well-defined with a large rmsd due to the absence of long-range NOEs (Figure 3). The binding of Ca^{2+} exposes B-helix to solvent and the hydrophobic interaction with the aromatic box becomes weaker (Figure 2). The similar alteration of the pattern of NOE cross-peaks in B-helix region was observed in the corresponding helix (F-helix) of the C-terminal domain of CaM (*45*). In the apo form, the position of C-helix is not well-defined compared with other helices. This is reflected by a small number of medium range NOEs and the absence of interhelical NOEs, suggesting looser hydrophobic packing than other helices. This feature is similar to C- and G-helices in CaM (*7*), and to the first helix of EF2 in TnC (*46*, *47*) and recoverin (*48*, *49*). On the other hand, C-helix in the Ca^{2+}-form of YCM0-N is well-defined as A- and D-helices. For CaM, C-helix is in a flexible conformation in the apo form; the hydrophobic interaction increases upon binding Ca^{2+}-ions (*2*, *50*).

Though the secondary structural elements of both structures of YCM0-N are almost the same, the orientations of B- and C-helix are remarkably different (Figure 2). Upon Ca^{2+} binding, hydrophobic residues are exposed to solvent and form a hydrophobic patch, which is assumed to be a binding part to target (Figure 5b). The total solvent-accessible area of YCM0-N in the apo and Ca^{2+}-saturated forms is almost the same with 5314 $\pm$ 115 and 5335 $\pm$ 96 $Å^2$, respectively. Solvent-accessible area of two Ca^{2+}-binding sites and C-helix region in the apo form is decreased by about 320 $Å^2$ in the Ca^{2+}-saturated form (Figure 3e). On the other hand, the solvent-exposed surface area for hydrophobic residues increases from 1094 $\pm$ 48 $Å^2$ in the apo form to 1479 $\pm$ 69 $Å^2$ in the Ca^{2+}-saturated form. This feature of YCM0-N agrees well with those of other EF-hand proteins that act as a Ca^{2+} sensor (*50*).

Ca^{2+}-Binding. YCM0-N has unusual amino acids in the two Ca^{2+}-binding loops. At the fourth position in EF1, Gly, the most common residue at this position (*38*) is replaced with Asn23 in YCM0-N, and φ and ψ angles of the Ca^{2+}-form are 56.3 $\pm$ 12.1 and 23.9 $\pm$ 7.3°, respectively, which is similar to 58 and 36° for Gly23. The invariant Gly at the sixth position (*52*) is replaced with His61 in EF2 of YCM0-N, and φ and ψ angles of the apo form are −128.2 $\pm$ 51.9

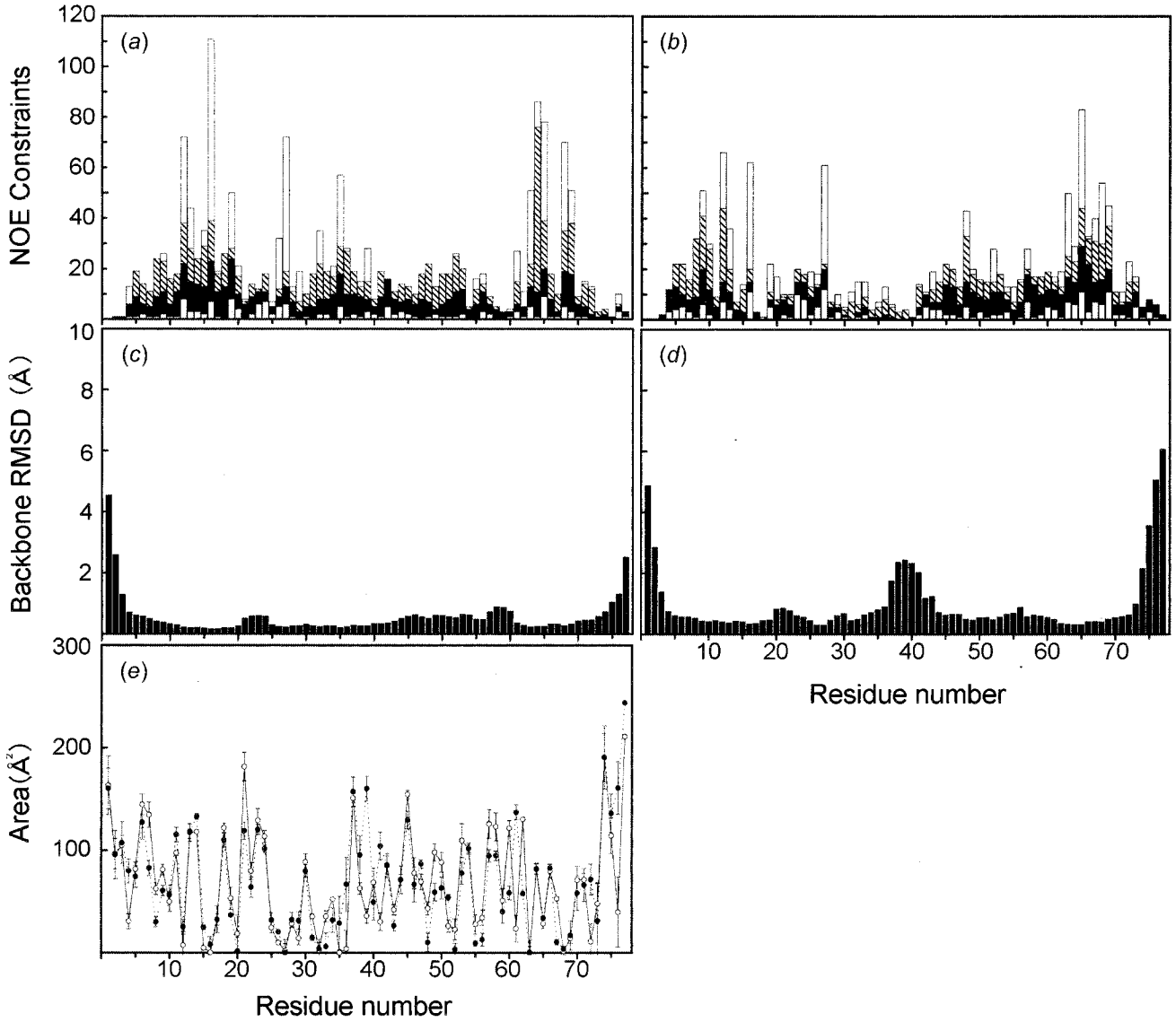

FIGURE 3: Structural data for apo YCM0-N and Ca^{2+}-saturated YCM0-N plotted as a function of residue number. NOE distribution for the apo (a) and Ca^{2+}-saturated forms (b). Intraresidue NOEs, sequential NOEs, medium range NOEs including NOEs (*i*,*i*+2), (*i*,*i*+3), and (*i*,*i*+4), and long-range NOEs are indicated by gray, black, slashed, and white bars, respectively. Values of rmsd of backbone heavy atoms (N, C_α, C, and O) for 30 apo (c), and Ca^{2+}-saturated forms (d). (e), Solvent accessible surface area of the apo (open circles connected by solid line) and the Ca^{2+}-saturated forms (filled circles connected by dotted line).

and 166.5 ± 4.3°, and those of the Ca^{2+}-form are 64.3 ± 3.5 and 10.4 ± 4.4°, respectively, instead of 90 and 0° for Gly61. Compared with the flexible Ca^{2+}-binding loops in apo CaM (*7*), the loop conformation of YCM0-N is comparatively well defined (Figure 3c). This result may be caused by reduced flexibility due to replacements of the two Gly residues in the loop. The imidazole ring of His61 close to C-helix is fixed around where Ca^{2+} would be accommodated (Figure 4a). It is known that charged side-chains are frequently located near the termini of α-helices (*53*, *54*). In the case of barnase, a model of the electrostatic interaction between the imidazole ring of His18 and the last turn of helix has been discussed (*55*). In our structure of the apo form, $N^{\epsilon 2}$ of His61 is located near the last turn of C-helix. NOE cross-peaks between the ring protons of His61 and the side-chains locating around C-terminal end of C-helix (Ile55, Asp56, and Val57) were identified. The electrostatic interaction between imidazole ring of His61 and C-helix may contribute to stabilizing the conformation of YCM0-N. The side chain of His61 is located in the inside of the second loop in the apo form, and it moves to the outside in the Ca^{2+}-binding form (Figure 4). As a result, NOE cross-peaks between the ring protons of His61 and residues of C-helix found in the apo form were not identified in the Ca^{2+}-form. Considering the stabilization of the second loop in the apo-form, EF2 of YCM0-N possibly functions as the low-affinity Ca^{2+}-binding site and the first Ca^{2+} binding occurs in EF1 of YCM0-N.

We reported that the affinity for Ca^{2+} of YCM0-N is significantly higher than that of the N-terminal domain of CaM, and the high affinity for Ca^{2+} is associated with a higher cooperativity in Ca^{2+} binding (*20*). It has been considered that the cooperative Ca^{2+} binding of CaM results from the concerted movement of helix pairs connected by a short linker region: B-helix of EF1 and C-helix of EF2 in the N-domain, and F-helix of EF3 and G-helix of EF4 in the C-domain (*7*). The cooperativity is not so high in the N-domain of CaM compared with that in the C-domain of

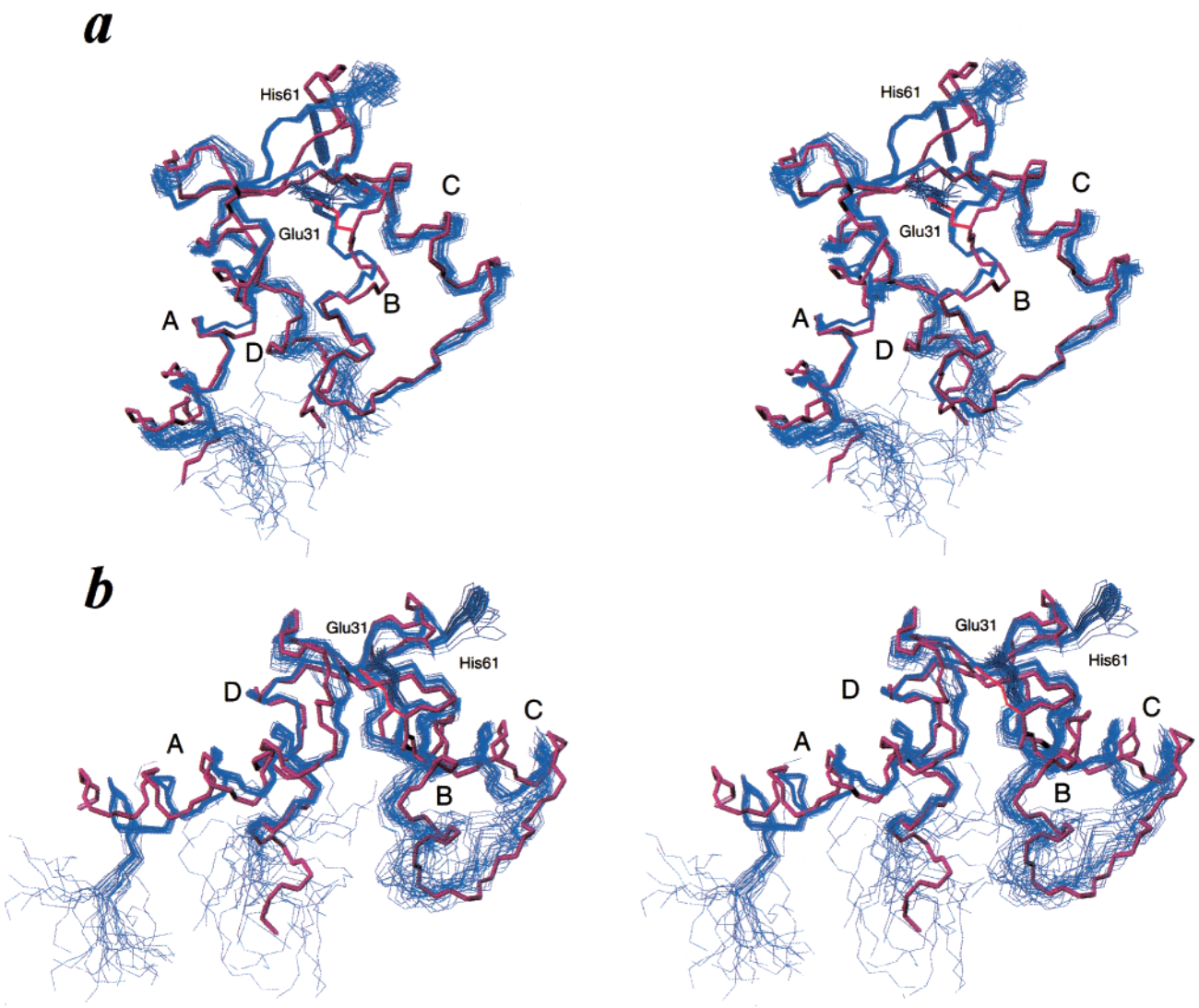

FIGURE 4: Comparison of the backbone conformation of YCM0-N with the N-domain of CaM (stereoviews). Comparisons of the N-domain of apo CaM (PDB accession number 1CFD) (red) with apo YCM0-N (blue) (a), and the N-domain of Ca^{2+}-saturated CaM (PDB accession number 3CLN) (red) with Ca^{2+}-saturated YCM0-N (blue) (b). 30 NMR conformers of apo and Ca^{2+}-saturated YCM0-N were superimposed on to the average structure of apo CaM and X-ray structure of Ca^{2+}-saturated CaM, respectively, using the backbone heavy atoms of residue 6−72. The side chains of Glu31 and His61 are also shown. Helices are labeled as described in the text.

CaM (*20*, *56*). Since the overall structure of apo YCM0-N is quite similar to that of the N-domain of apo CaM, small structural differences between them may be important to increase the affinity of Ca^{2+} for YCM0-N. In addition to the similar Ca^{2+}-dependent rearrangement of the B- and C-helix pair of YCM0-N (Figure 2), the following structural feature may be important for the highly cooperative Ca^{2+} binding to YCM0-N. As shown in Figure 4a, the β-sheet of apo YCM0-N is remarkably twisted as compared to the counterpart of CaM, which reflects low sequence similarity of this region to CaM (Figure 1). The φ angles of Ser26, Ile27, and Ser28 in the first β-strand are -139.3 ± 3.9, -131.5 ± 7.2, and $-82.2 \pm 8.6°$, respectively. On the other hand, the φ angles of corresponding residues of CaM are -139.6 ± 0.6, -140.2 ± 0.1, and $-90.0 \pm 2.0°$, respectively. Gln62, Ile63, and Glu64 are residues of the second β-strand and whose φ angles are -99.2 ± 5.3, -71.9 ± 3.2, and $-120.0 \pm 6.5°$, respectively. On the other hand, the φ angles of corresponding residues of CaM are -138.4 ± 2.8, -140.2 ± 0.1, and $-101.6 \pm 1.1°$, respectively. A twisted β-sheet in apo YCM0-N changed to a slightly twisted conformation as a result of Ca^{2+} binding (Figure 4). As a result, the φ and ψ angles of the residues in the β-sheet of YCM0-N are almost the same as those of CaM in the Ca^{2+}-form. The amide proton of Ile27 in the first strand of β-sheet, which forms a hydrogen bond with Ile63, shows a notably large low-field shift from 8.18 ppm in the apo form to 9.77 ppm in the Ca^{2+}-form probably due to the enhanced hydrogen bonding in the β-sheet. The amide proton of Ile63, which forms another hydrogen bond in the β-sheet, also shows a low-field shift. A similar observation was reported in Mg^{2+}- and Ca^{2+}-forms of YCM0-N (*22*). The β-sheet of the C-domain of CaM, to which Ca^{2+} binds with high cooperativity, is also highly twisted in the apo form, and Ca^{2+} binding removes this twist (*1*, *2*, *6*, *7*, *45*). Therefore, this conformational change in the β-sheet may play an important role for the cooperative Ca^{2+} binding, by which Ca^{2+} binding in one EF-hand can affect the other EF-hand to form the Ca^{2+}-binding conformation.

As discussed in the previous paragraph, Ca^{2+} is thought to bind first to EF1 of YCM0-N. Then the following reorientation of C-helix by the concerted movement of B-

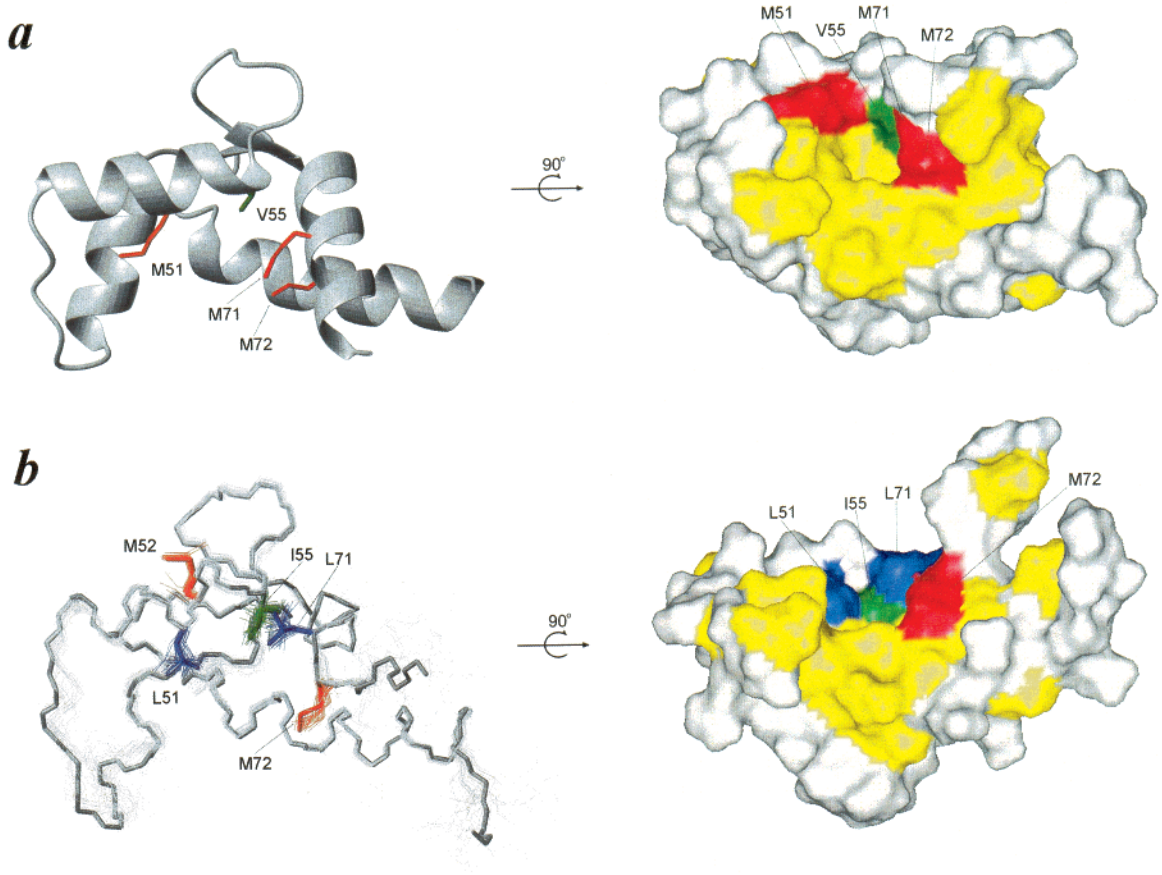

FIGURE 5: (a) Ribbon diagrams and surface structure of the N-domain of Ca^{2+}-saturated CaM (PDB accession number 3CLN). (b, left) Backbone atoms of 30 NMR structures (thin lines) of Ca^{2+}-saturated YCM0-N superimposed on the energy-minimized their average conformation (thick line). (b, right) Surface structure of the average conformation of Ca^{2+}-saturated YCM0-N. All Mets except for ill-determined Met36 and Met76 are shown in red. Leu51 and Leu71 of YCM0-N are shown in blue. Residues of position 55 in both proteins are shown in green. In surface structures, other hydrophobic residues are shown in yellow.

and C-helices reduces the electrostatic interaction between the side chain of His61 and C-helix, which was discussed in the previous paragraph, due to increase in the distance between them. The lower interaction energy may result in easy replacement of the side chain of His61 with Ca^{2+} in EF2. It might also contribute to the highly cooperative Ca^{2+} binding in YCM0-N.

For apo CaM, the N-terminal part of B-helix (residues 29−31) forms 3_{10}-helix and has a kink at the position of Glu31 (*6*, *7*). On the other hand, B-helix of YCM0-N is a regular α-helix throughout this region. The observed twist in the *β*-sheet is probably responsible for this difference. The similar discussion was reported for the C-domain of CaM (*6*). As a result, the position of Glu31 in apo YCM0-N is a little different from that of CaM (Figure 4a). However, the position of Glu31 in the Ca^{2+}-form is almost the same as that of CaM (Figure 4b). Thus, the rsmd values for C_α of Glu31 between apo and Ca^{2+}-saturated CaM and between those of YCM0-N are 3.37 ± 0.06 and 2.89 ± 0.19 Å, respectively, when the loop regions (residues 20−31) were superimposed. The smaller movement of Glu31 of YCM0-N than that of CaM seems to be one of reasons for the high Ca^{2+}-affinity of YCM0-N.

Target Binding. CaM activates various Ca^{2+}-dependent enzymes by recognizing the CaM-binding domains of target enzymes (*8*−*11*). On the other hand these target enzymes of vertebrate CaM are activated only to limited levels by YCM0 (*19*, *21*). Since the hydrophobic surfaces exposed in each domain of CaM are responsible for the activation by recognizing the diverse sequences of CaM-binding domain of targets, the exposed hydrophobic surface of YCM0-N were compared with the corresponding region of CaM (Figure 5). The hydrophobic surface in each domain of CaM is rich in Met residue (four residues in each domain) with a flexible hydrophobic side chain, and Met51 and Met71 collaborating with Met36 and Met72 in the N-domain of CaM have been considered to be essential for matching the hydrophobic surface to a diversity of hydrophobic anchor residues in the CaM-binding domain (*12*−*15*). YCM0-N has four Met (Met36, Met52, Met72, and Met76) and positions of Met52 and Met72 were defined (Figure 5b). Met36 on ill-converged region of B-helix and Met76 in the C-terminal region were not defined and were excluded in Figure 5b. Met52 in YCM0-N corresponding to Ile52 in CaM is located in a different position to stabilize C-helix through a hydrophobic interaction with Leu32, which is inferred from NOE cross-peaks between Met52 and Leu32. Met51 and Met71 in CaM are replaced with Leu in YCM0-N, which has a more rigid and larger side chain, and they are exposed to solvent on Ca^{2+} binding (Figure 3e). Val55 in CaM, another constituent which interacts with the anchor residue of target is replaced with Ile55 in YCM0-N (Figures 1 and 5). Thus side chains of Leu51, Leu71, and Ile55 in place of Met51, Met71, and Val55 of CaM may directly interact with the anchor residue

of target enzymes on the exposed hydrophobic surface of YCM0-N. As a result, YCM0-N has a less flexible and smaller hydrophobic pocket than that of the N-domain of CaM, which may restrict an acceptable volume of anchor residue (Figure 5b). The feature of the exposed hydrophobic surface may account for limited levels of activation of target enzymes, or restricted diversity in target recognition of YCM0-N (*18*, *21*).

Since three Met out of four in the C-domain of CaM are also replaced with Leu in the C-domain of YCM0, the C-domain of YCM0 also may have a less flexible and small hydrophobic pocket. Thus YCM0 may bind target with two of less flexible and smaller hydrophobic pockets than those of CaM. The CaM binding sequences of sk- and smMLCK belong to the same classification in the distribution of electric charges and the interval of anchor residue (12 residues) (*11*) and bind to CaM with an antiparallel orientation: the N- and C-terminal anchor residues bind to hydrophobic pockets of the C- and N-domain of CaM, respectively. The N-terminal anchor residue is Trp in both MLCKs, and the C-terminal anchor residue is Phe for skMLCK and Leu for smMLCK. The activation constants (K_{act}) of YCM0 are more than 17000-fold for skMLCK and more than 600-fold for smMLCK, compared with those of CaM (*58*), which may be at least partly attributed to the too much bulky anchor residue for proper accommodation in the hydrophobic surfaces of YCM0 with restricted flexibility. YCM0 is also a poor activator of the 120-kDa brain PDE (*58*), which also has Trp as the N-terminal anchor (*59*, *60*). So far target enzymes with Trp as the anchor residue are not found in yeast (*15*, *61*). The reported K_{act} values of YCM0 for yeast CaN and CaMKI are within nanomolar range (*57*; K.N. and M.Y., unpublished result). The N-terminal anchor residue of CaMKI from rat and human is Trp, whereas it is replaced with Phe in yeast CaMKI (*61*). On the basis of the same classification, the C-terminal anchor residue of yeast CaN is Val, and the residue of yeast CaMKI or CaMKII is Leu, both of which may well conform to the hydrophobic pocket with restricted flexibility in the N-terminal domain of YCM0. Further, vertebrate CaN with Val as the C-terminal anchor can be efficiently activated by YCM0 with a similar affinity for CaM (K.N. and M.Y., unpublished results). Therefore, the volume of anchor residue may influence the affinities of target enzymes for YCM0. The replacements of Met51, Met71, and Val55 in CaM with Leu51, Leu71, and Ile55 in YCM0 may be one of important factors that restrict a volume of side chain of anchor residue in the N-terminal domain.

REFERENCES

1. Babu, Y. S., Bugg, C. E., and Cook, W. J. (1988) *J. Mol. Biol. 204*, 191−204.
2. Babu, Y. S., Sack, J. S., Greenhough, T. J., Bugg, C. E., Means, A. R., Cook, W. J. (1985) *Nature 315*, 37−40.
3. Kawasaki, H., and Kretsinger, R. H. (1994) Protein Profile *1*, 343−346.
4. Barbato, G., Ikura, M., Kay, L. E., Pastor, R. W., and Bax, A. (1992) *Biochemistry 31*, 5269−5278.
5. Tjandra, N., Kuboniwa, H., Ren, H., and Bax, A. (1995) *Eur. J. Biochem. 230*, 1014−1024.
6. Kuboniwa, H., Tjandra, N., Grzesiek, S., Ren, H., Klee, C. B., and Bax, A. (1995) *Nat. Struct. Biol. 2*, 768−776.
7. Zhang, M., Tanaka, T., and Ikura, M. (1995) *Nat. Struct. Biol. 2*, 758−767.
8. Ikura, M., Clore, G. M., Gronenborn, A. M., Zhu, G., Klee, C. B., and Bax, A. (1992) *Science 256*, 632−638.
9. Meador, W. E., Means, A. R., and Quiocho, F. A. (1992) *Science 257*, 1251−1255.
10. Meador, W. E., Means, A. R., and Quiocho, F. A. (1993) *Science 262*, 1718−1721.
11. Osawa, M., Tokumitsu, H., Swindells, M. B., Kurihara, H., Orita, M., Shibanuma, T., Furuya, T., and Ikura, M. (1999) *Nat. Struct. Biol. 6*, 819−824.
12. Vogel, H. J. (1994) *Biochem. Cell Biol. 72*, 357−376.
13. Siivari, K., Zhang, M., Palmer, A. G., III, and Vogel, H. J. (1995) *FEBS Lett. 366*, 104−108.
14. Gellman, S. H. (1991) *Biochemistry 30*, 6633−6636.
15. Cyert, M. S., Kunisawa, R., Kaim, D., and Thorner, J. (1991) *Proc. Natl. Acad. Sci. U.S.A. 88*, 7376−7380
16. Klee, C. B., and Vanamann, T. C. (1982) *Adv. Protein Chem. 35*, 213−321.
17. Davis, T. N., Urdea, M. S., Masiarz, F. R., and Thorner, J. (1986) *Cell 47*, 423−431.
18. Luan, Y., Matsuura, I., Yazawa, M., Nakamura, T., and Yagi, K. (1987) *J. Biochem. 102*, 1531−1537.
19. Starovasnik, M. A., Davis, T. N. and Klevit, R. E. (1993) *Biochemistry 32*, 3261−3270.
20. Nakashima, K., Ishida, H., Ohki, S., Hikichi, K., and Yazawa, M. (1999) *Biochemistry 38*, 98−104.
21. Ohya, Y., Uno, I., Ishikawa, T., and Anraku, Y. (1987) *Eur. J. Biochem. 168*, 13−19.
22. Ohki, S., Miura, K., Saito, M., Nakashima, K., Maekawa, H., Yazawa, M., Tsuda, S., and Hikichi, K. (1996) *J. Biochem. 119*, 1045−1055.
23. Matsuura, I., Ishihara, K., Nakai, Y., Yazawa, M., Toda, H., and Yagi, K. (1991) *J. Biochem. 109*, 190−197.
24. Matsuura, I., Kimura, E., Tai, K., and Yazawa, M. (1993) *J. Biol. Chem. 268*, 13267−13273.
25. Schleif, R. F., and Wensink, P. C. (1981) *Practical Methods in Molecular Biology*, p 197, Springer-Verlag, New York.
26. Yazawa. M., Sakuma, M., and Yagi, K. (1980) *J. Biochem. 87*, 1313−1320.
27. Rance, M., Sørensen, O. W., Bodenhausen, G., Wagner, G., Ernst, R. R., and Wüthrich, K. (1983) *Biochem. Biophys. Res. Commun. 117*, 479−485.
28. Jeener, J., Meier, B. H., Bachmann, P., and Ernst, R. R. (1979) *J. Chem. Phys. 71*, 4546−4553.
29. Macura, S., and Ernst, R. R. (1980) *Mol. Phys. 41*, 95−117.
30. Braunschweiler, L., and Ernst, R. R. (1983) *J. Magn. Reson. 53*, 521−528.
31. Davis, D. G., and Bax, A. (1985) *J. Am. Chem. Soc. 107*, 2820−2821.
32. Morris, G. A., and Freeman, R. (1978) *J. Magn. Reson. 29*, 433−470.
33. Piotto, M., Saudek, V., and Sklenár, V. (1992) *J. Biomol. NMR, 2*, 661−665.
34. Kay, L. E., Keifer, P., and Saarinen, T. (1992) *J. Am. Chem. Soc. 114*, 10663−10665.
35. Kay, L. E., Marion, D., and Bax, A. (1989) *J. Magn. Reson. 84*, 72−84.
36. Marion, D., Driscoll, P. C., Kay, L. E., Wingfield, P. T., Bax, A., Gronenborn, A. M., and Clore, G. M. (1989) *Biochemistry 28*, 6150−6156.
37. Delaglio, F., Grzesiek, S., Vuister, G. W., Zhu, G., Pfeifer, J., and Bax, A. (1995) *J. Biomol. NMR 6*, 277−293.
38. Strynadka, H. C. J., and James, M. N. G. (1989) *Annu. Rev. Biochem. 58*, 951−998.
39. Brünger, A. T. (1992) *X-PLOR Manual*, Yale University Press, Cambridge, MA, version 3.1.
40. Nilges, M., Clore, G. M., and Gronenborn, A. M. (1988) *FEBS Lett. 229*, 317−324.
41. Koradi, R., Billeter, M., and Wüthrich, K. (1996) *J. Mol. Graphics 14*, 51−55.
42. Chazin, W. J., and Wright, P. E. (1988) *J. Mol. Biol. 202*, 603−622.
43. Morris, A. L., MacArthur, M. W., Hutchinson, E. G., and Thornton, J. M. (1992) *Proteins 12*, 345−364.

44. Kabsch, W., and Sander, C. (1983) *Biopolymers 22*, 2577−2637.
45. Finn, B. E., Evenäs, J., Drakenberg, T., Waltho, J. P., Thulin, E., and Forsén, S. (1995) *Nat. Struct. Biol. 2*, 777−783.
46. Findlay, W. A., and Sykes, B. D. (1993) *Biochemistry 32*, 3461−3467.
47. Gagné, S. M., Tsuda, S., Li, M. X., Smillie, L. B., and Sykes, B. D. (1995) *Nat. Struct. Biol. 2*, 784−789.
48. Ames, J. B., Tanaka, T., Stryer, L., and Ikura, M. (1994) *Biochemistry 33*, 10743−10753.
49. Tanaka, T., Ames, J. B., Harvey, T. S., Stryer, L., and Ikura, M. (1995) *Nature 376*, 444−447.
50. Kretsinger, R. H., Rudnick, S. E., and Weissman, L. J. (1986) *J. Inorg. Biochem. 28*, 289−302.
51. Ikura, M. (1996) *Trends Biochem. Sci. 21*, 14−17.
52. Marsden, B. J., Shaw, G. S., and Sykes, B. D. (1990) *Biochem. Cell Biol. 68*, 587−601.
53. Presta, L. G., and Rose, G. D. (1988) *Science 240*, 1632−1641.
54. Richardson, J. S., and Richardson, D. C. (1988) *Science 240*, 1648−1652.
55. Sancho, J., Serrano, L., and Fersht, A. R. (1992) *Biochemistry 31*, 2253−2258.
56. Minowa, O., and Yagi, K. (1984) *J. Biochem. 96*, 1175−1182.
57. Okano, H., Cyert, M. S., and Ohya, Y. (1998) *J. Biol. Chem. 273*, 26375−26382.
58. Nakashima, K., Maekawa, H., and Yazawa, M. (1996) *Biochemistry 35*, 5602−5610.
59. Barth, A., Martin, S. R., and Bayley, P. M. (1998) *Biopolymers 45*, 493−501.
60. Yuan, T., Walsh, M. P., Sutherland, C., Fabian, H., and Vogel, H. J. (1999) *Biochemistry 38*, 1446−1455.
61. Ohya, Y., Kawasaki, H., Suzuki, K., Londesborough, J., and Anraku, Y. (1991) *J. Biol. Chem. 266*, 12784−12794.

BI000582X